

CO-Induced Restructuring on Stepped Pt Surfaces: A Molecular Dynamics Study

Joseph R. Michalka,^{†,‡} Andrew P. Latham,[†] and J. Daniel Gezelter^{*,†}

[†]*Department of Chemistry and Biochemistry*

University of Notre Dame

251 Nieuwland Science Hall

Notre Dame, Indiana 46556

[‡]*Department of Chemistry and Physics*

Southwest Baptist University

Wheeler Science Facility

Bolivar, Missouri 65613

E-mail: gezelter@nd.edu

Phone: (574) 631-7595

Abstract

The effects of plateau width and step edge kinking on carbon monoxide (CO)-induced restructuring of platinum surfaces were explored using molecular dynamics (MD) simulations. Platinum crystals displaying four different vicinal surfaces [(321), (765), (112), and (557)] were constructed and exposed to partial coverages of carbon monoxide. Platinum-CO interactions were fit to recent experimental data and density functional theory (DFT) calculations, providing a classical interaction model that captures the atop binding preference on Pt. The differences in Pt–Pt binding strength between edge atoms on the various facets were found to play a significant role in step edge wandering and reconstruction events. Because the mechanism for step doubling relies on a stochastic meeting of two wandering edges, the widths of the plateaus on the original surfaces was also found to play a role in these reconstructions. On the Pt(321) surfaces, the CO adsorbate was found to assist in reordering the kinked step edges into straight {100} edge segments.

Introduction

Industrial catalysts often consist of supported metal nanoparticles or high-index metal surfaces. Both of these materials have a high density of undercoordinated atoms which have been shown to be active for catalytic reactions.¹⁻⁴ Catalytic activity on low-energy metal surfaces, primarily the (111), (110), and (100) facets, is only indirectly applicable to industrial conditions.⁵⁻⁸ With new experimental techniques like high pressure scanning tunneling microscopy (HP-STM) and ambient pressure X-ray photoelectron spectroscopy (AP-XPS), high index surfaces can now be explored at higher temperatures and pressures. This allows for a more complete understanding of the surface structures of industrial catalysts.⁹⁻¹¹ Roughened surfaces and nanoparticles are of particular interest because morphology and stability at high temperatures and pressures depends on the presence and identity of adsorbates.¹²⁻¹⁸ Under reaction conditions, many of these catalysts have also been observed to reconstruct, drastically changing the surface of the catalyst and altering the activity and selectivity of the material.¹⁷⁻¹⁹

Carbon monoxide (CO) oxidation on platinum (Pt) surfaces has been studied extensively as a model catalyst. One system that has received significant attention is the Pt(557) surface.^{13-15,17} Tao *et al.*, using HP-STM, AP-XPS, and density functional theory (DFT) calculations, observed that by introducing CO to the system, the stepped Pt surface would undergo a step-doubling reconstruction yielding steps that were twice as high and plateaus that were twice as wide as the original surface.¹³ If the system was maintained at these conditions, the appearance of triangular nanoclusters bridging the steps were also observed. After removing CO from the system, it was found that these changes were reversible, as the Pt(557) surface was recovered. It was suggested that this reconstruction was caused by the strong repulsive interactions between adsorbed CO molecules. This system has also been explored with molecular dynamics simulations where a possible mechanism, involving the large CO-CO quadrupolar repulsion from adjacent atop adsorption sites near step edges, was proposed to explain the step-doubling process.¹⁵

The strong interaction of CO with Pt has been explored on different systems and similar results have been observed. Ferrer *et al.*, examining Pt(997), observed both O and CO induced step-

doubling on the surface. They also saw that the presence of step-doubling was correlated with a factor of three increase for CO oxidation rates.¹⁹ Park *et al.*, again exploring the Pt(557) system exposed to CO, saw that the ordering of the triangular nanoclusters is very sensitive to temperature and can undergo its own reversible restructuring separate from the doubling already observed on this surface.¹⁷

Similarly, Eren *et al.* found that a flat Cu(111) surface, when exposed to CO, also underwent significant reconstruction, forming small nanoclusters on the surface that were highly active for the oxygen reduction reaction (ORR).¹⁸ In all of these cases, the presence of adsorbates led to large-scale reconstructions (often reversible) of the surface. However, the dependence of the reconstruction dynamics on the originally displayed surface structure is still unclear.

This paper attempts to answer the question of how initial surface morphology affects reconstruction pathways by examining the effect of CO on the reconstruction of various Pt facets, specifically focusing on the effect of edge type and plateau width. The Pt(321),^{20–22} Pt(112),^{23,24} Pt(765), and Pt(557)^{13,15,16,25} vicinal surfaces were chosen as they represent a mixture of straight and kinked atomic steps as well as narrow and wide plateaus. Based on the proposed mechanism in Ref. 15, it is hypothesized that the width of the plateau and the roughness of the step edge will both contribute to the reconstruction on these surfaces. These systems were modeled using classical force fields that balance chemical accuracy with computational efficiency. At room temperature, the structural changes occur on timescales of 10–100s, so molecular dynamics simulations with elevated temperatures are necessary to observe the evolution of these systems.

Methodology

Modeling surface reconstructions of solid/gas interfaces requires relatively large systems and long timescales. To observe events such as step doubling and step wandering, systems need to contain on the order of 10^3 – 10^4 atoms that are observed for tens to hundreds of nanoseconds. The large number of electrons associated with metallic interfaces makes modeling these interfaces with

ab initio molecular dynamics (AIMD),^{26–28} Car-Parrinello methods,^{29–31} or quantum mechanical potential energy surfaces intractable. However, the interactions between metal atoms are poorly represented by pairwise interactions. Therefore, the Embedded Atom Method (EAM)³² was used to model the Pt–Pt interactions as it can effectively handle large numbers of atoms while including non-pairwise effects. For modeling CO, a three site model developed by Straub and Karplus was utilized.³³ This model treats the CO as a rigid body and was chosen primarily for its accurate description of the large linear quadrupole of CO. The Pt–CO interaction was modeled to match a combination of recent experimental^{5,34,35} and theoretical^{36–41} data.

Platinum-Platinum Interactions

Since force fields with only pairwise interactions do not treat transition metal cohesive energies correctly, several methods have been developed that describe metallic interactions utilizing non-pairwise additive functions of the local electron density. Some of these methods include the embedded atom (EAM),^{32,42–48} the Finnis-Sinclair^{49,50} and the quantum-corrected Sutton-Chen methods.⁵¹ In general, these methods treat a metal atom as a positive core surrounded by a radially decaying charge density representing the valence electrons. Computing the energy for placing atom i in a specific location requires computation of the electron density contributed by all other metallic atoms in the system,

$$\rho_i = \sum_{j \neq i} \rho_j(r_{ij}). \quad (1)$$

$\rho_j(r_{ij})$ is the valence electron density contributed by atom j at site i . The potential energy of atom i is provided by a functional, $F_i[\rho_i]$, which describes the attractive energy between the positive core of the atom and the background electron density contributed by the surrounding metal,

$$V_i = F_i[\rho_i] + \sum_{j \neq i} \phi_{ij}(r_{ij}), \quad (2)$$

while $\phi_{ij}(r_{ij})$ represents the pairwise repulsion between the positively charged cores. Potentials similar to the forms in Eqs. (1) and (2) are used in the EAM, Finnis-Sinclair, and Quantum Sut-

ton Chen models. These models have been used for a variety of theoretical calculations of bulk and nanoparticle properties,^{52–55} melting,^{56–58} fracture,^{59–61} crack propagation,⁶² and alloying dynamics.^{63–66} As the EAM parameterization includes second and third nearest-neighbor interactions, it is particularly suited to interfaces that deviate from low-energy (111) surfaces, and the “u3” EAM fits are utilized in this work.³²

Surface Models

Vicinal Pt surfaces were generated by slicing an ideal FCC lattice along planes corresponding to specific Miller indices (hkl). Two perpendicular cuts were used to generate an orthorhombic slab, and the desired plane was oriented along the z axis of the simulation box, which is periodic in all three dimensions. For each of the simulated surfaces, Pt(321), Pt(112), Pt(765), and Pt(557), ideal surfaces were doubled in either the x or the y direction. These systems are identified as LS, for systems with longer steps, and MS, for systems with more steps. The system dimensions, number of atoms, and number of surface atoms are enumerated in Table 1. In each case, the box was extended along the z -axis to a length of 100 Å to allow for a sufficient gas phase layer between periodic replicas of the system. Note that each simulation cell displays two of the $\{hkl\}$ facets to the gas, one in the positive z direction and one facing the negative z axis.

Surface energies were calculated for every system that was studied, as well as for the low-index Pt(111), Pt(100), and Pt(110) surfaces. To perform these calculations, systems were created such that they were periodic in all directions (x, y, z). The desired surface was then exposed by extending the box in the z -direction a sufficient distance to prevent long-range interactions between the exposed facets. The change in the potential energy that resulted was used to calculate the surface energy. The surface energies calculated for the low-index surfaces match previous values calculated using the same potential.³² Note that for the low-index facets, these values are a factor of ~ 1.3 larger than surface energies obtained via experiments^{67–69} and DFT,⁷⁰ but the ratios of surface energies are preserved relative to experimental ratios. The EAM surface energies for the higher index facets are also shown in Table 1, and by analogy with the low index facets, these are

Table 1: Surface Models

Pt Surface	Atoms	Surface Atoms	dimensions (Å)		Slab thickness (Å)	Surface Energy (J/m ²)	Plateau Width (Å)
			MS	LS			
(321)	4440	720	71.7 × 47.7	35.8 × 95.5	18.85	1.76	5.90
(112)	4608	768	32.9 × 108.5	65.8 × 54.3	18.40	1.67	6.79
(557)	3888	720	110.6 × 24.8	55.3 × 49.5	18.52	1.55	13.79
(765)	3744	792	28.7 × 100.5	58.4 × 50.2	19.24	1.53	16.79

expected to be a factor of 1.3 larger than experimental surface energies for the same facets. We note that the surface energies of these systems are inversely correlated with the plateau widths. Larger plateaus correspond to larger regions of exposed low energy (111) facets.

Carbon Monoxide

The large linear quadrupole moment of CO is believed to play a role in the reconstruction of Pt(557).^{13,15} The model of Karplus and Straub effectively reproduces that quadrupole.³³ This model consists of a rigid body comprising three sites. Two sites describe the C and O, both with a partial negative charge, while the third site (M) is massless and carries a large neutralizing positive charge. The M site is located at the center of mass of the molecule. The parameters for this model are shown in Table 2. These parameters produce a molecule with a small dipole moment (0.35 D) while keeping the linear quadrupole (-2.40 DÅ) close to both experimental calculations (-2.63 DÅ)⁷¹ and quantum mechanical predictions (-2.46 DÅ).⁷²

Table 2: Positions, Lennard-Jones parameters (σ and ϵ) and charges for CO–CO interactions

	z (Å)	σ (Å)	ϵ (kcal/mol)	q (e^-)
C	-0.6457	3.83	0.0262	-0.75
O	0.4843	3.12	0.1591	-0.85
M	0.0			1.6

Platinum-Carbon Monoxide Interactions

Extensive experimental^{5,17,34,35,73,74} and theoretical^{36–41} work on Pt–CO systems allows for significant data for parameterizing a force field for the Pt–CO interaction. The Pt–CO model used here has evolved from our previous models^{15,16} in order to improve the difference in energy between the preferred atop and bridge sites described by recent DFT calculations.³⁶ The current model uses a repulsive Morse potential to represent the Pt–O interaction, while previous implementations have used a standard “shifted” Morse potentials.^{15,37} The repulsive Morse potential

prevents unphysical O-first binding to the surface. Combining the Lennard-Jones Pt–C interaction with the repulsive Morse model for the Pt–O interaction, the resulting potential,

$$V_{\text{PtCO}} = 4\varepsilon \left(\left(\frac{\sigma}{r_{\text{PtC}}} \right)^{12} - \left(\frac{\sigma}{r_{\text{PtC}}} \right)^6 \right) + D_e e^{-2\gamma(r_{\text{PtO}} - r_e)}. \quad (3)$$

Table 3 shows the parameters for the Pt-CO interaction, while Table 4 provides the binding energies for the various (111) binding sites based on these parameters and compares them to DFT³⁶ and experimental data.^{5,35}

Table 3: Parameters for Pt-CO Interaction

Pt-C	
σ	1.68 Å
ε	52.25 kcal / mol
Pt-O	
r_e	5.15 Å
D_e	0.03 kcal/mol
γ	1.7 Å ⁻¹

Table 4: Pt-CO Binding Site Preferences (eV)

	Atop	Bridge	Hollow
This work	-1.49	-1.36	-1.32
DFT ³⁶	-1.48	-1.47	-1.45
Experimental ^{5,35}	-1.43		

Simulation Protocol

The bare interfaces were run in the canonical (NVT) ensemble, where the temperature was gradually raised to either 700 K for Pt(321) or 1000 K for Pt(112), Pt(765), and Pt(557). Systems with wider plateaus are significantly more stable and were run at 1000 K to bring reconstruction dynamics into the domain of typical simulation times. In the STM papers (Refs. 13 and 17), CO was present at pressures between 5×10^{-9} and 1.05 Torr, yielding coverages between 0.5 and 1 ML. In our simulations, gas phase CO molecules, corresponding to 0.25 ML or 0.5 ML of surface coverage

were placed in the vacuum region and then allowed to adsorb on the surface. The dosed systems were re-equilibrated for one nanosecond before data collection. Data was collected by running the systems in the microcanonical (NVE) ensemble for 100 ns. Simulations were performed using the open source molecular dynamics package, OpenMD.^{75,76}

Generalized coordination number

For many catalytic reactions, only a subset of the atoms on a roughened surface or nanoparticle are catalytically active. While the coordination numbers of individual atoms can describe their binding strengths, Calle-Vallejo *et al.* observed that including the first and second nearest neighbor counts allowed for a more complete description of an atom's local environment and its catalytic activity.⁷⁷ They introduced the *generalized coordination number* (GCN), to describe this quantity,

$$\overline{CN}(i) = \sum_{j=1}^{n_i} \frac{cn(j)}{cn_{\max}} \quad (4)$$

The GCN is an extension of nearest-neighbor analysis where the GCN of atom i , $\overline{CN}(i)$, is calculated from the average of the coordination numbers, $cn(j)$, of atom i 's nearest neighbors (j). The sum is carried out over atom i 's first solvation shell, and cn_{\max} is a normalization term. For an FCC crystal, $cn_{\max} = 12$, the bulk coordination number. The concept is further illustrated in Figure 1 where we see an ideal Pt(321) surface color coded to match the computed GCN values. The bulk atoms (GCN=12) make up the majority of the system. However, there is a wide range of potentially catalytically active sites on the surface. Calle-Vallejo *et al.* argued that for the Oxygen Reduction Reaction (ORR) a Pt atom with a GCN of ~ 8.3 would be the most catalytically active site. Since an ideal (111) surface is composed of atoms with a GCN of $7.5 = (6 \times 9 + 3 \times 12)/12$, this implies that surfaces that display some amount of concavity may be necessary to achieve the highest catalytic activities. The GCN distribution for an ideal Pt (557) system is included in the Supporting Information as Fig. S1 to highlight the differences between kinked (321) edges and the flat edges of the (557) surface.

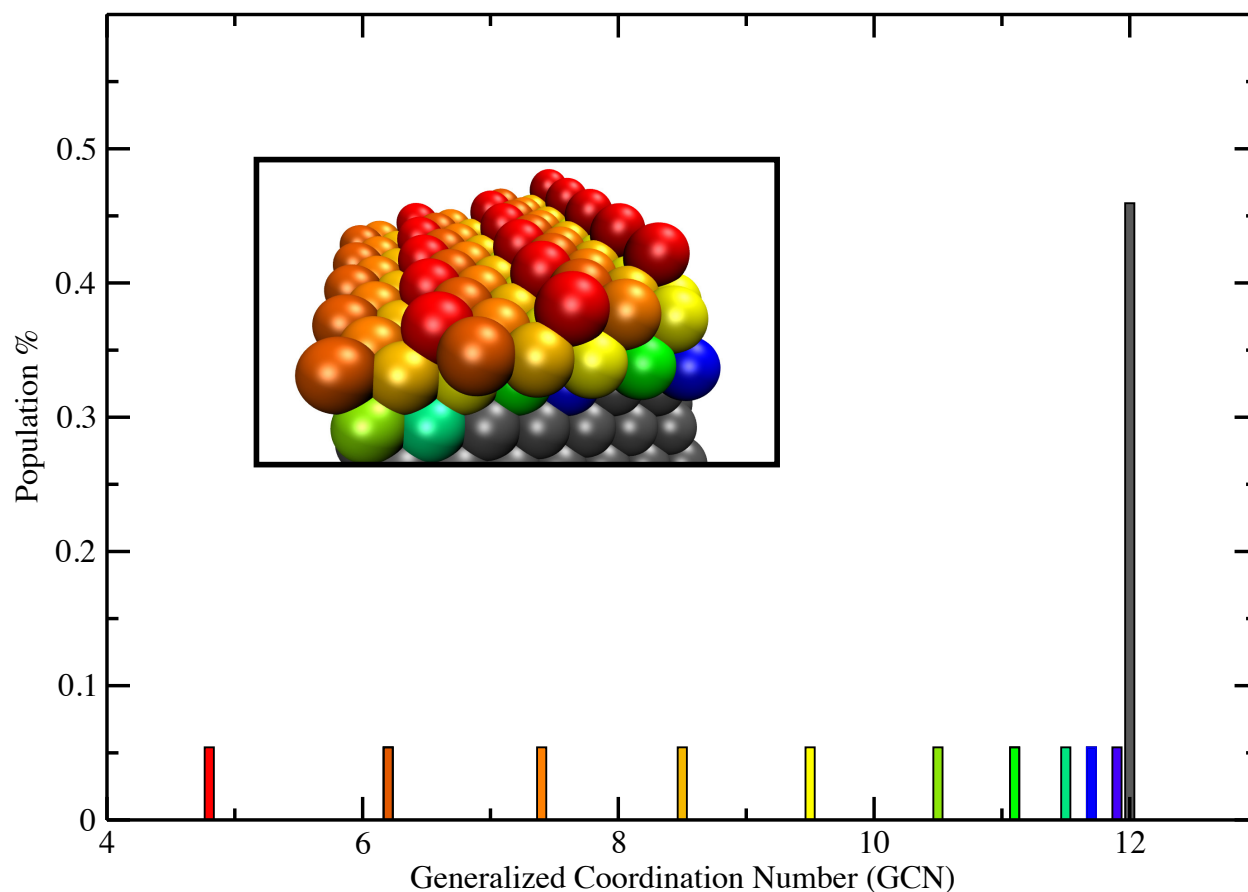


Figure 1: The generalized coordination number of an ideal Pt (321) system colored to match the inset structure. Other than the bulk (GCN = 12), the ideal (321) surface displays a wide variety of coordination environments at its surface. The under-coordinated edge atoms (red) have the lowest GCN, where the plateau atoms have GCN values around the ideal (111) surface number of 7.5. Subsurface atoms (yellow, greens, and blues) have a larger GCN than the surface, but are still less coordinated than the bulk.

Step-edge detection

Because individual steps on the metal surface display the low energy (111) facet, our method for identifying atoms in step edges divides the bulk metallic system into a series of (111) planes. We make use of the Miller indices (hkl) of the initial interface, *e.g.* (557) which have been oriented to sit perpendicularly to the z -axis of the simulation cell. The vector normal to the (111) plateaus defines an angle that the plateaus make with the simulation cell (see fig. 2),

$$\cos(\theta) = \frac{h+k+\ell}{\sqrt{3(h^2+k^2+\ell^2)}} \quad (5)$$

The surfaces were constructed with the initial step edge lying along either the x - or y -axes, so one of the two vector components is zero. If the system has the initial step edge oriented along the y -axis, the vector normal to the (111) plateaus is

$$\mathbf{v}_{111} = \begin{pmatrix} \sin \theta \\ 0 \\ \cos \theta \end{pmatrix}. \quad (6)$$

Atoms are assigned to a plateau by projecting their instantaneous coordinates onto the (111) normal vector, $v_i = \mathbf{r}_i \cdot \mathbf{v}_{111}$. Histograms of these projections allow separation of the (111) planes, and each atom is assigned to a plateau using the instantaneous v_i values.

If the initial step edge runs parallel to the y -axis, we may define a new vector that is perpendicular to both the step edge and the (111)-normal,

$$\mathbf{u}_{111} = \mathbf{v}_{111} \times \hat{\mathbf{y}} \quad (7)$$

The locations of atoms within a single (111) plane are transformed into the new coordinate system with basis vectors $\{\mathbf{u}_{111}, \hat{\mathbf{y}}, \mathbf{v}_{111}\}$. For a given value of the $\hat{\mathbf{y}}$ coordinate, it is relatively straightforward to find the atoms with the minimum and maximum values along the \mathbf{u}_{111} coordi-

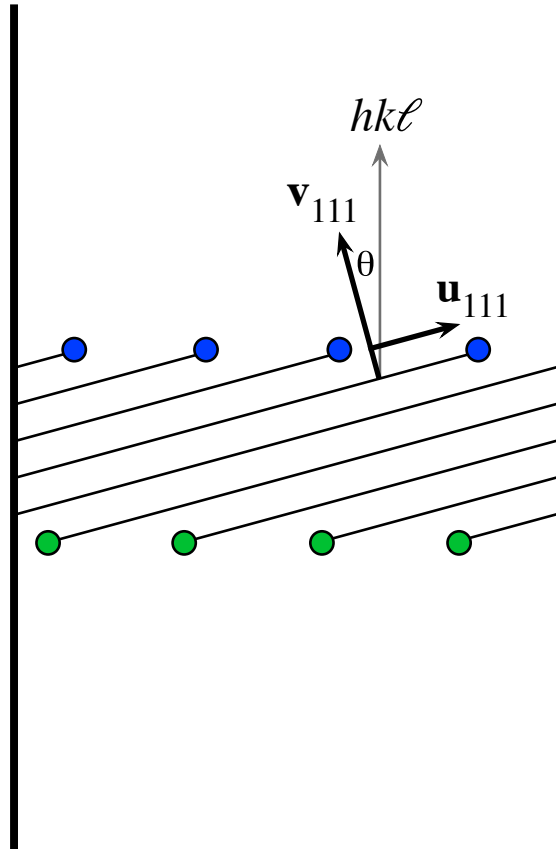


Figure 2: Projection of the hkl normal vector onto the (111) normal vector (\mathbf{v}_{111}) to find an angle (θ) for the tilt of the step edges relative to the box geometry. Step edge atoms are defined by the maximum and minimum \mathbf{u}_{111} values on each plateau plane. The step edges project into the plane of the figure.

nate. These atoms are shown with blue and green dots in fig. 2.

In periodic boundary conditions, each of the (111) plateaus exhibits two edges in the simulation cell, and the top and bottom edge atoms are collected separately and sorted by their \hat{y} values. This list of atoms is a single “edge” that can be followed dynamically and analyzed over the course of a trajectory.

Results

Changes in surface coordination

In Figure 3, we show the generalized coordination distribution from the Pt(321) systems which have been limited to the surface and subsurface layers, i.e. non-bulk, for three CO coverages at both the beginning and end of the simulations. The growth in the peaks around 7.5, highlighted with a blue bar, suggests that the surface has undergone reconstruction resulting in larger (111) domains on the surface. The amount of CO present in the system plays a direct role in this reconstruction. The loss of height in peaks at GCN ~ 4.5 and ~ 6.2 suggest that these systems are reconstructing by displaying more of the lower energy (111) facets. The growth in GCN near 11.2 indicates that the subsurface layers are becoming more bulk-like.

While the majority of the other surfaces examined in this study experienced significantly less reconstruction, the Pt(112) LS systems did exhibit both edge wandering and reconstruction. Figure 4 shows the evolution of GCNs for the Pt(112) LS systems. There is a similar reduction of population around GCN ~ 4.5 and 5.5 which is consistent with both reconstruction and step *sinking*. The increased peak heights at 6.5, 7.4, and 8.5 indicate a CO-induced flattening of the surface. Representative GCN plots of the other interfaces are included in the SI as Figures S2 through S4.

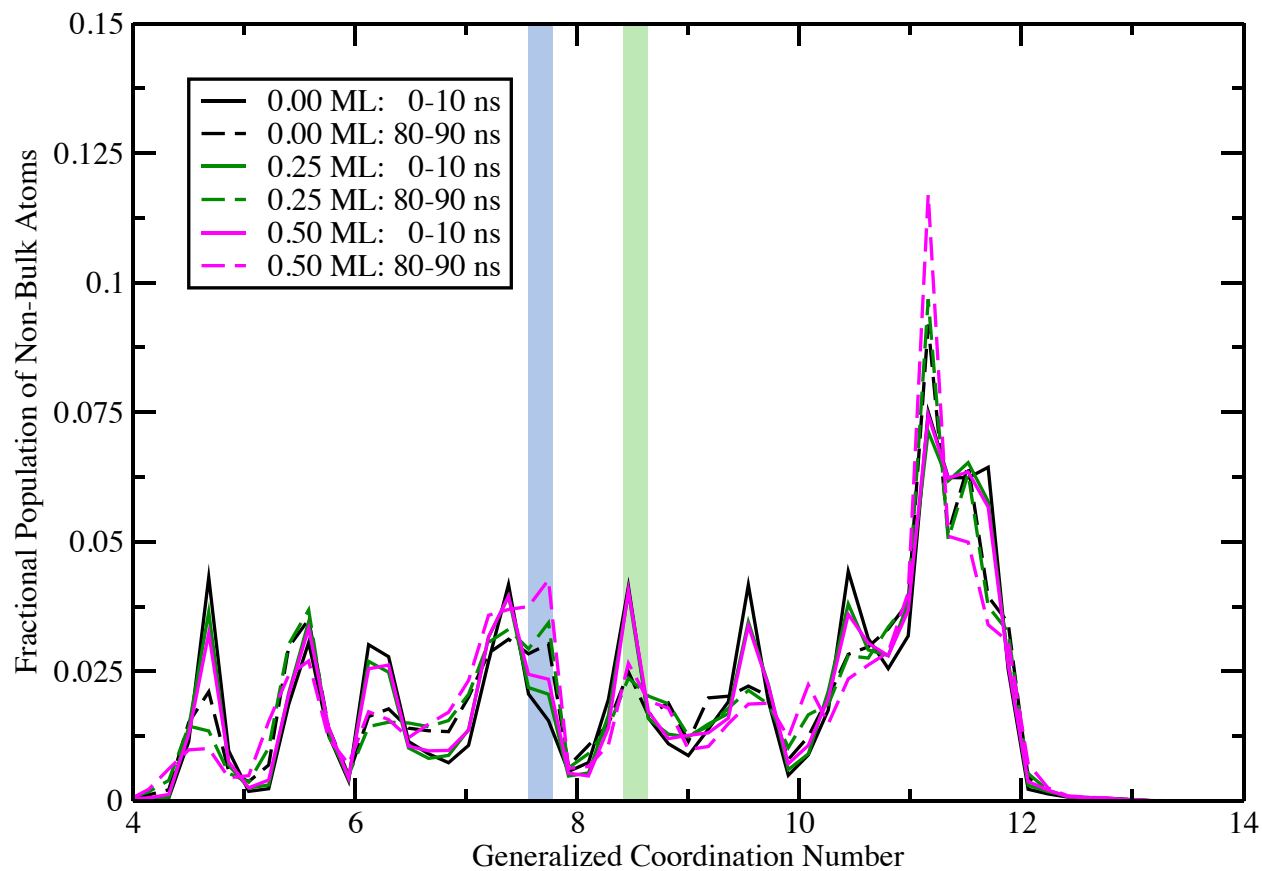


Figure 3: The distribution of generalized coordination numbers (GCN) for the near-surface atoms of the Pt(321) LS systems. Solid lines represent the averaged GCN during the first 10 ns of simulation time, while dashed lines correspond to the last 10 ns. The undosed surface (black) exhibits moderate reconstruction, while the 0.25 ML (green) and 0.50 ML (magenta) show significantly more evolution towards (111) plateaus. The blue bar is aligned with GCN \sim 7.5 which corresponds to surface atoms in an ideal Pt (111) surface, while the green bar highlights the region identified by Calle-Vallejo *et al.* as being especially active for ORR activity.⁷⁷

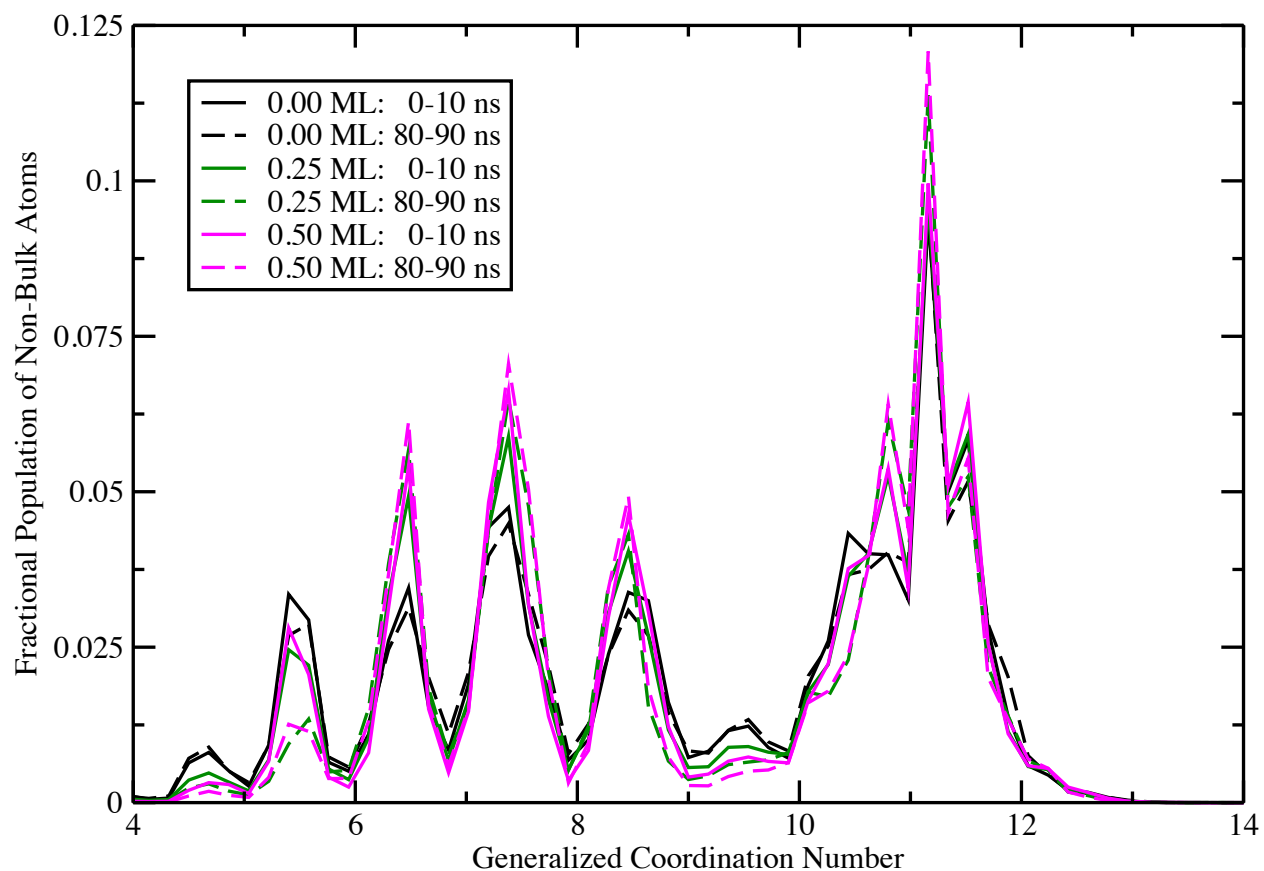


Figure 4: The distribution of GCN values for the near-surface atoms of the Pt(112) LS systems. Colors and line styles are the the same as Fig. 3. There is a notable loss of population at GCN ~ 4.5 and 5.5 on the CO-dosed surfaces and corresponding increases at 6.5 , 7.4 , and 8.5 . These changes point to a CO-induced flattening of the Pt(112) surface.

Edge wandering

Pt (557)

The Pt(557) surfaces have been explored more fully in previous experimental and theoretical work,^{13,15} but the step doubling appears to be sensitive to the details of the Pt-CO interaction. As in previous simulations, there were numerous instances of edge wandering. In this work, however, no doubling nucleation sites formed on the (557) surfaces, although they were seen previously in Ref. 15. Our Pt-CO interaction has been reduced in binding strength compared with the previous work, and this may have reduced the driving force for step doubling. It is also possible that nucleation of the doubling reconstruction is a relatively rare event, and 100 ns of simulation time is insufficient to observe the doubling on Pt(557) at this temperature.

Pt (112)

The Pt(112) MS surfaces exhibited a small amount of CO-induced restructuring, although this interface exhibits a mode of releasing surface tension in which some of the {100} step edges sink into the surface, shifting sideways to display a “sunken” or lowered {111} step edge. This is highlighted in Figure S5 in the SI. Adatom formation from the sunken steps was minimal and the total adatom movement on these systems was reduced compared with interfaces with wider plateaus.

The Pt(112) LS surfaces exhibited significant step-wandering, along with a moderate amount of edge reconstruction. About half of the steps on each system sank into the bulk, preventing most adatom formation, but the remaining steps were active sources of adatoms and edge wandering. Step doubling was observed for the 0.25 ML and 0.5 ML surfaces. Figure 5 highlights the 0.25 ML LS system and the step doubling that was observed, along with the sinking of other step edges on the surface.

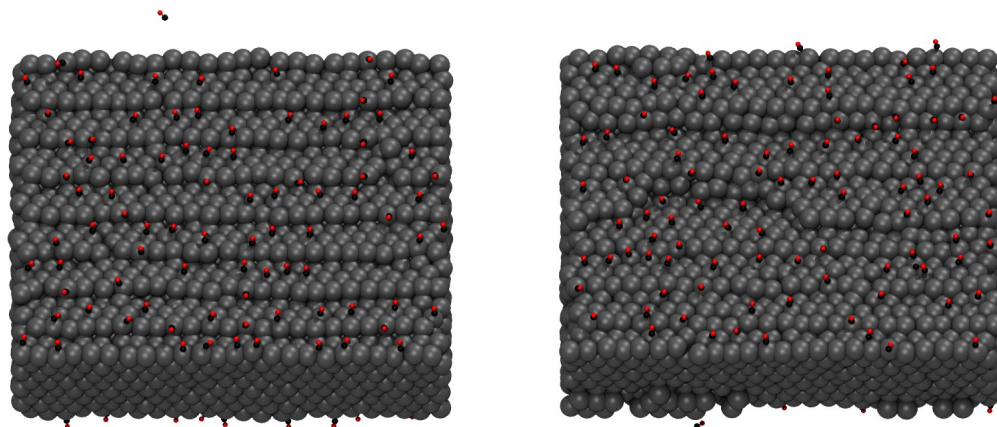


Figure 5: The Pt(112) 0.25 ML LS surface. At the beginning of the simulation (left), minimal step-wandering has occurred. Step doubling (near the top of the right panel) and edge sinking (near the bottom) both play a role in lowering the surface energy of this system.

Pt (765)

The Pt(765) surfaces, while undergoing significant step-wandering, did not exhibit step doubling during the simulations. The MS systems (those extended to display more steps) maintained the (765) motif over the entire simulation. What appeared to be the initial stages of a doubling event resulted in portions of the two edges sinking into the surface of the metal.

The LS systems also experienced significant step wandering. While no doubling was observed, connections between separate edges were seen. However, these connections led to step rotation on the surface of the metal. Despite the apparent stability of the (765) motif for the MS systems, the 0 and 0.5 ML LS systems underwent a relatively unstructured surface morphology change. Notably, there is an increase in the GCN population near 6.8 highlighted in Figure S4 in the SI.

Pt (321)

The small plateau widths and kinked step edges on the Pt(321) surface showed the most interesting behavior after exposure to CO. Numerous step-doubling events were observed on both the MS and LS systems with 0.5 ML CO. The 0.25 ML systems also showed significant reconstruction, although fewer step doubling events were observed. At the relatively high temperatures used in this study, the 0 ML systems also experienced a small amount of step wandering.

An interesting case of frustrated double layer formation is highlighted in Figure 6 where three double layers have nucleated, but the doubling highlighted in green is preventing both the blue and red double layers from coalescing. Within the 100 ns encompassed by the simulations, the 0.5 ML LS systems were not able to form a double step that traversed the length of the system, while numerous examples of partial or frustrated double steps were found.

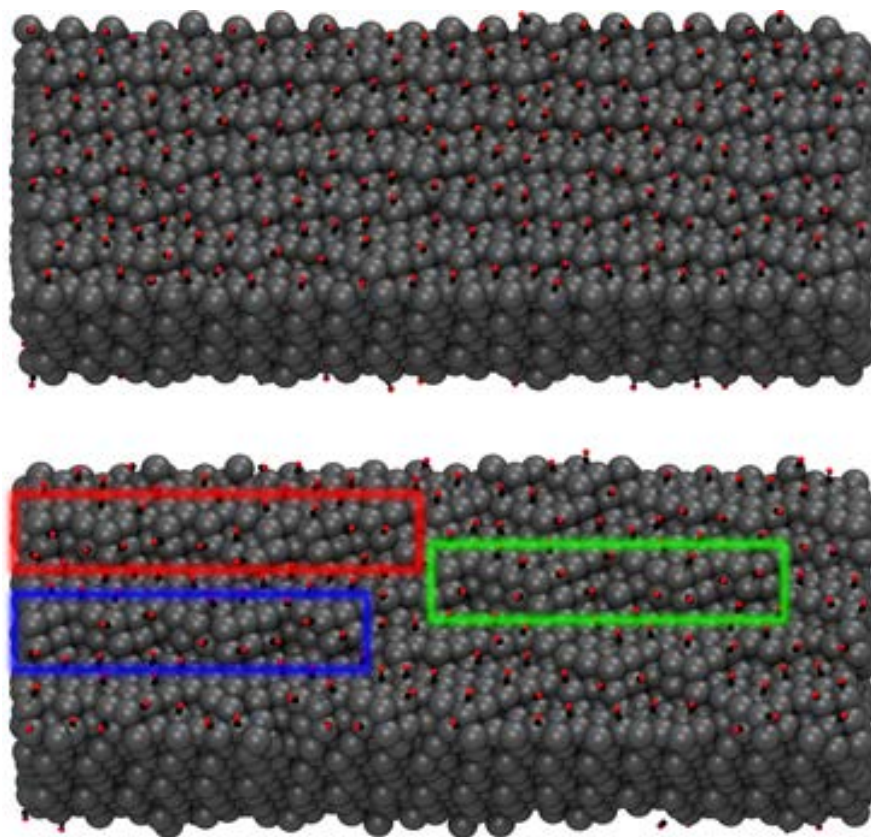


Figure 6: The Pt(321) 0.5 ML LS system. Immediately after dosing with CO (top), the kinked edges are stable. By 100 ns after dosing, the adsorbed CO has induced double step formation. The plateaus are sufficiently narrow that the formation of double step nucleation sites can happen in many locations. Zippering of the double layers completes a reconstruction on other surfaces, but is hindered by the presence of a nascent double layer on an adjacent step. Frustrated double layers were common on this surface.

At a lower CO coverage (0.25 ML), the Pt(321) surface exhibited the structure highlighted in Figure 7. There is a small degree of step-edge doubling in these systems, but the majority of this surface exhibited diamond shaped (111) domains.

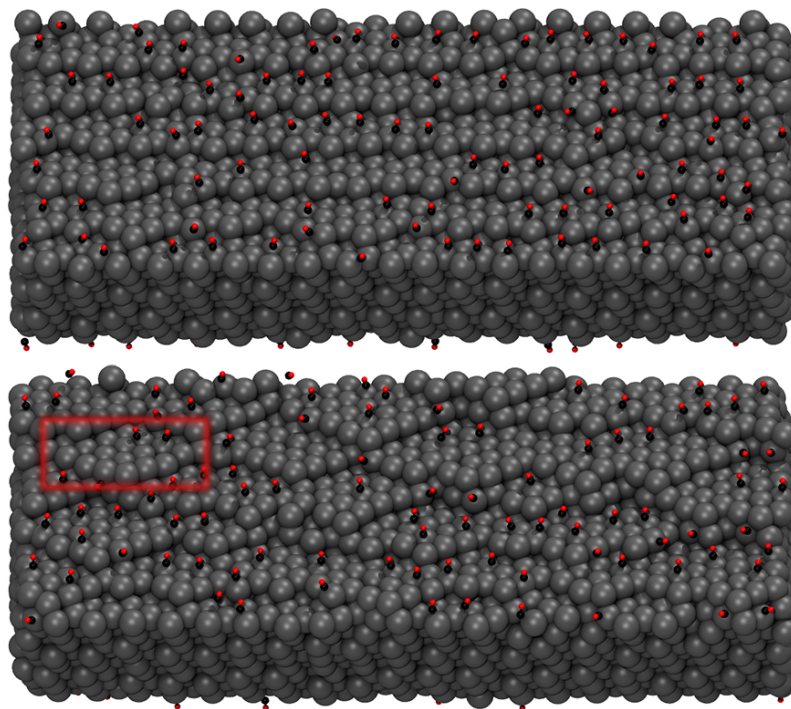


Figure 7: The Pt(321) 0.25 ML LS system. Immediately after dosing (top) the kinked edges are stable. After 100ns (bottom), the red box highlights one of the repeated (111) “diamond” domains formed between the initially regular steps.

Discussion

Plateau width

On these stepped surfaces, the width of the (111) plateaus provides a good estimate of the surface energy of the facet. The plateau width also has an effect on the mechanism of restructuring. The doubling mechanism proposed in Ref. 15 depends on two step edges meeting and forming a stable nucleation site. After nucleation, a zippering process accelerates the rest of the step reconstruction. Because the meeting of two step edges is a stochastic process, any feature that makes the initial meeting less likely, e.g. increasing the distance between edges, will make the reconstruction process more difficult to capture in reasonable simulation times.

Conversely, a small plateau width should increase the number of nucleation events, which should in turn lead to increased step doubling. Both the (321) and (112) systems show evidence of this. The Pt(112) LS systems experienced four clear instances of step doubling – two on the 0.25

ML LS system, and two on the 0.5 ML LS system – all of which were completed within the first 27 ns of the simulations. The Pt(321) systems, while exhibiting partial double layers, often appeared in a frustrated configuration, and only three full ($> 95\%$) doublings were observed during the simulations. While the process of step doubling on the (112) systems occurred fairly smoothly, the doubling of the (321) surfaces did not. The diamond motifs highlighted in Figure 7 were stable for the majority of the simulation. In the instances where the diamonds broke apart, this was followed by an adjacent step doubling within ~ 5 ns. Thus, despite nucleation sites forming rapidly on the (321) surfaces, the stability of these sites slowed or even prevented the step doubling process from going to completion.

Energy to separate from an edge

Adatom creation is essential for step wandering and doubling. To show the effects of CO adsorbates on this process, we have computed potential energies for adatom creation under several CO configurations.^{15,16} These energy surfaces were computed by displacing one Pt edge atom along the plateau in a direction perpendicular to the step edge (shown in Figs. 8 and 9). The strong quadrupolar repulsion between bound CO molecules makes adatom formation energetically favorable at high coverages. For the (112) and (557) facets, configurations *e*, *g*, and *h*, shown in Fig. 8, make the initial formation of an adatom an energetically favorable process. Because the step edges are kinked in the (321) and (765) facets, more CO configurations (*e*, *f*, *g*, and *h*) are favorable for adatom formation (see Fig. 9).

This analysis provides several useful bits of data. First, removing an atom from a (321) or (765) step is more energetically favorable than from a (112) or (557) step. The former two facets have kinked step edges, which lower the coordination number for the edge atoms. This trend is clearly shown in Figures 8 and 9 for configuration *a* where no CO is present on the surface. In these instances, creating an adatom from a kinked step edge is 10 kcal/mol more favorable than from a flat step.

Additionally, the width of the plateaus affects the energy required to form an adatom at higher

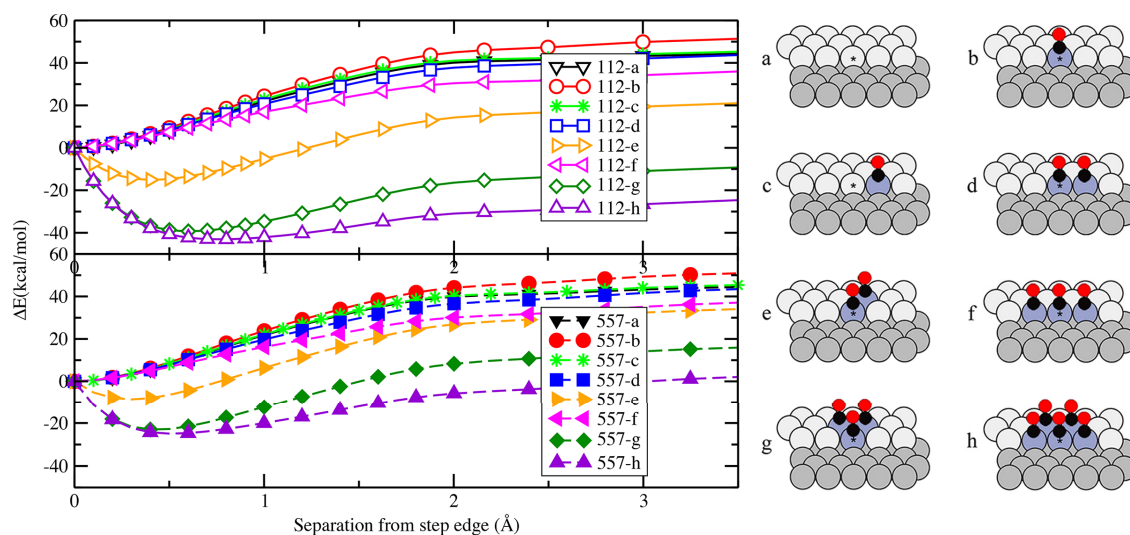


Figure 8: Energies for displacing an edge atom (*) perpendicularly from the (112) (top) and (557) (bottom) step edges. Each of the energy curves corresponds to one of the labeled configurations on the right and are referenced to the unperturbed step edge. The spheres represent Pt atoms on the upper (white) and lower (grey) steps. Colored atoms (blue) are depicted with a CO molecule adsorbed in an atop configuration. Certain configurations of CO, notably *e*, *g* and *h*, can lower the energetic barrier for creating an adatom.

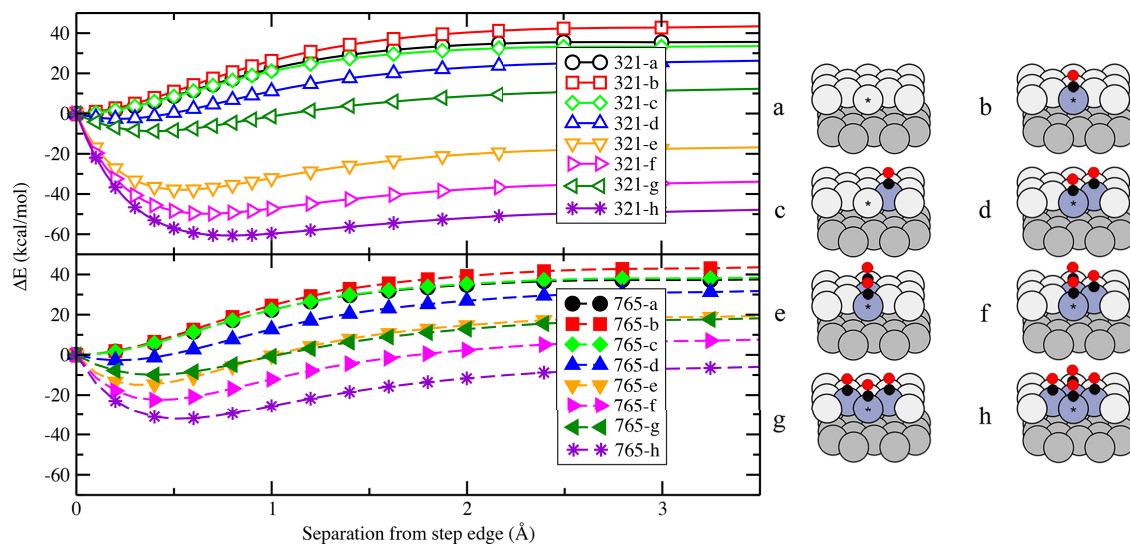


Figure 9: Energies for displacing an edge atom (*) perpendicularly from the (321) (top) and (765) (bottom) kinked step edges. The configurations to the right of the graphs show the kinked step edges of these facets. The kinked steps lower the energetic barrier for adatom creation when compared to the flat steps of the (112) and (557) surfaces. Plateau width also has a significant effect on the energetic benefit of adatom formation.

coverages. Configurations *e*, *f*, and *h* in Figure 9 for the kinked steps highlights this result. It is approximately 25 kcal/mol more favorable to form an adatom on the (321) surface than it is on the (765) surface. Similarly, there is approximately a 20 kcal/mol difference in favor of forming an adatom from a (112) step-edge when compared to the (557) surface.

Finally, the location and arrangement of CO strongly affects the energy required to remove the atom from the step edge. Separation becomes most favorable when the candidate adatom and the atom directly behind it both have an atop-adsorbed CO. This configuration directs the strong quadrupolar repulsion directly away from the step edge, lowering the barrier for adatom formation. Comparing configurations *d* and *e* in both figures illustrates this effect. In configuration *e*, both adsorbed CO molecules are situated along a line which is perpendicular to the step edge. In configuration *d* the repulsion due to the CO is mostly parallel to the step edge. As the coverage increases, the likelihood increases for observing one of the CO configurations conducive to adatom formation, thereby increasing Pt surface mobility.

Edge Ordering

The steps in the (321) facet were observed to change from kinked edges to larger {100} edge segments. After dosing with CO, the change in angular ordering of the steps was analyzed to track the straightness of step edges for all four facets. Assuming atoms $i - 1$, i , and $i + 1$ are sequential along a step edge, \mathbf{a}_i is defined as the vector between $i - 1$ and i and \mathbf{b}_i is the vector between i and $i + 1$. An effective measure of the ordering is,

$$\langle \cos^2 \theta \rangle = \left\langle \frac{1}{N_{\text{edge}}} \sum_i \left(\frac{\mathbf{a}_i \cdot \mathbf{b}_i}{|\mathbf{a}_i| |\mathbf{b}_i|} \right)^2 \right\rangle, \quad (8)$$

where the averaging is done over all of the edges present in a configuration. Here N_{edge} is the number of atoms present in the edge. Atoms in straight step edges would result in $\cos^2 \pi = 1$ while the ideal (321) kinked surface would result in $\cos^2 \left(\frac{2\pi}{3} \right) = 0.25$.

For the (321) facet, the systems start near the ideal $\cos^2 \theta = 0.25$ but quickly grow towards a

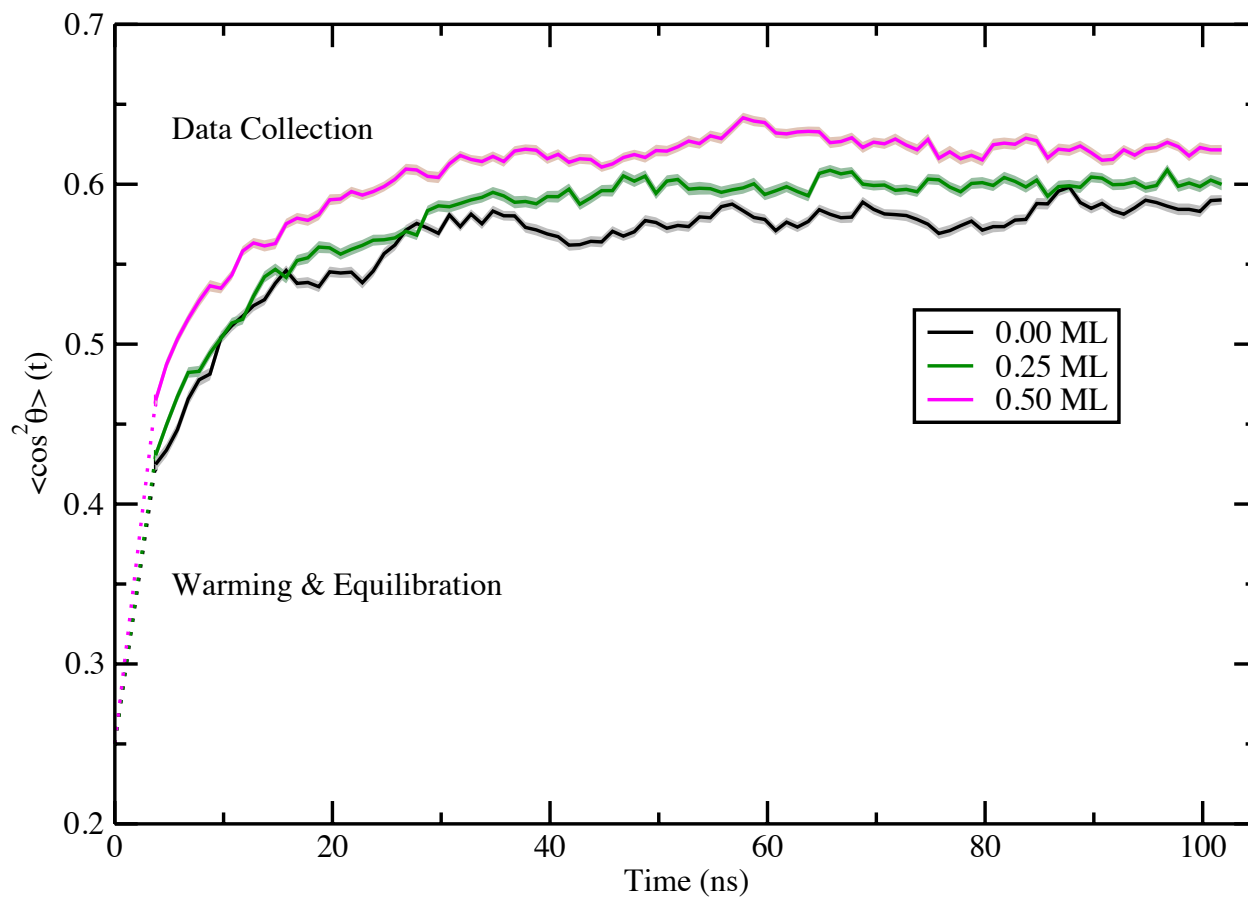


Figure 10: Evolution of the edge-ordering over time for the Pt(321) systems. Both the bare and CO-dosed surfaces start near the ideal $\langle \cos^2 \theta \rangle = 0.25$ and rapidly rise during the first 40 ns of the simulation. Generally, the presence of CO leads to increased linear ordering of the step-edges.

more ordered set of edges (see Fig. 10). Some ordering by CO coverage is observed, where the systems with CO tend to display more ordered edges. This appears to be due both to the lower energy of the $\{100\}$ edge segments and the CO-induced mobility of edge atoms.

Mechanisms of structural changes

Our previous work on Pt(557) revealed that adsorbed CO destabilizes the step-edges leading to rapid formation of adatoms and step-wandering on the surface. If sufficient step-wandering occurs, two step edges can connect to form a nucleation site. Once one of these sites is formed, a zippering of the double step across the length of the simulation cell happens rapidly.

This mechanism depends on the stochastic meeting of two step edges which is correlated with the density of metal adatoms on the surface. Thermal energy can increase the number of adatoms, however in the current work, this pathway is limited due to lower simulation temperatures. The systems without CO, while exhibiting some adatom formation and re-absorption, showed minimal reconstruction. When CO was introduced, moderate surface reconstruction was observed. The presence of CO plays a similar role to increased temperature by weakening the Pt–Pt bonds along the step-edge.

Besides the density of adatoms, another factor in step edge wandering is the plateau width. The narrow plateaus in the (112) and (321) systems makes step edge meetings more likely. In previous work on the (557) surface, only one nucleation site was necessary for a step doubling. For many of the surfaces explored in this study, many nucleation sites are created before the steps complete the doubling. In some cases, this leads to frustrated doubling, highlighted in Fig. 6.

All of the (321) surfaces, even those without CO present, showed some amount of surface roughening and reconstruction suggesting that these surfaces have limited stability at high temperatures. However, the presence of 0.25 and 0.5 ML coverages of CO did lead to significantly more step-wandering, intermediate reconstructions, and partial and full double layer formation.

Summary

The mechanism and dynamics of reconstruction on Pt surfaces, specifically step doubling, depends on the displayed surface facet. It is also dependent on the presence of adsorbates, here CO, that can disrupt the step-edges and then stabilize the formation of double steps. The energetics of step-edge breakup shows that the kinked surfaces, (321) and (765), are especially favorable for formation of adatoms due to undercoordination of the edge atoms.

The mechanism proposed in our earlier work involving stochastic edge-doubling nucleation followed by zippering is mostly supported by the current work. Specifically, systems with narrower plateaus form frustrated double layers because multiple nucleation sites form before zippering can be completed.

Re-parameterization of the Pt–CO interaction to match new experimental and DFT binding energies has altered the dynamics of the step-doubling process, particularly for the (557) surfaces. While significant step-wandering was observed on Pt(557), the density of adatoms was not sufficient to form nucleation sites during the 100 ns simulation time.

One notable new finding is the observation that on the (321) facet, the CO adsorbate can assist in restructuring the kinked step edge into longer segments of straight $\{100\}$ edges. With high CO coverages, the kink atoms are highly susceptible to ejection from the edge, but they can add to a straight segment with a lower energetic penalty. This energetic argument indicates that kinked steps, like the ones exhibited by the Pt(321) and Pt(765) surfaces, should be most susceptible to CO-induced reconstruction.

The cell formed by step-edge atoms may also play a role in the dynamics of reconstruction. Tao *et al.*,¹³ examining both the Pt(557) surface that exhibits a (100) step edge and the Pt(332) surface that exhibits a (111) edge, observed that the extent and final structure of the CO-induced reconstruction were affected by the type of step edge. The Pt(557) surface showed a significant degree of reconstruction at low pressures, and was observed to form triangular nanoclusters at high coverages. The Pt(332) surface exhibited less reconstruction at low CO coverages and formed rectangular nanoclusters at high coverages. Investigation of the detailed molecular dynamics of

(100)-edge surfaces like Pt(332) will increase our ability to predict the dynamics of reconstruction on these surfaces, and will be the topic of future study.

Recent work on CO-induced nanostructure formation on a Cu(111) surface has shown that when the metal-metal binding interactions are weaker, the presence of strong repulsive adsorbates can be sufficient to disrupt even flat surfaces.¹⁸ We have reached a similar conclusion with the Pt systems in our simulations. Surfaces that have a higher surface energy and more sites where adatoms can be easily formed are more likely to experience reconstruction in general. In particular, step doubling increases the fraction of the surface that is occupied by the low surface-energy (111) domains.

Supporting Information

The Supporting Information includes: GCN data for an additional ideal surface (Pt(557)) to complement the Pt(321) surface in Fig. 1, distributions of GCN values for the Pt(557) LS and Pt(765) systems, Pt(112) step edge configurations, and sunken edge illustrations for the Pt(765) system.

Acknowledgement

Support for this project was provided by the National Science Foundation under grant CHE-1362211 and by the Center for Sustainable Energy at Notre Dame (cSEND). Computational time was provided by the Center for Research Computing (CRC) at the University of Notre Dame.

References

- (1) Jeong, H.-C.; Williams, E. D. Steps on surfaces: experiment and theory. *Surf. Sci. Rep.* **1999**, *34*, 171 – 294.
- (2) Larsen, J. H.; Chorkendorff, I. From fundamental studies of reactivity on single crystals to the design of catalysts. *Surf. Sci. Rep.* **1999**, *35*, 163 – 222.
- (3) Shi, H.; Auerbach, S. M.; Ramasubramaniam, A. First-Principles Predictions of Structure–Function Relationships of Graphene-Supported Platinum Nanoclusters. *J. Phys. Chem. C* **2016**, *120*, 11899–11909.
- (4) Tao, F. F.; Crozier, P. A. Atomic-Scale Observations of Catalyst Structures under Reaction Conditions and during Catalysis. *Chem. Rev.* **2016**,
- (5) Ertl, G.; Neumann, M.; Streit, K. Chemisorption of CO on the Pt(111) Surface. *Surf. Sci.* **1977**, *64*, 393–410.
- (6) Levine, S.; Garofalini, S. Molecular dynamics simulation of atomic O on Pt(111). *Surf. Sci.* **1986**, *167*, 198 – 206.
- (7) Wong, Y. T.; Hoffmann, R. Chemisorption of carbon monoxide on three metal surfaces: nickel(111), palladium(111), and platinum(111): a comparative study. *J. Phys. Chem.* **1991**, *95*, 859–867.
- (8) Greeley, J.; Nørskov, J. K.; Mavrikakis, M. Electronic Structure and Catalysis on Metal Surfaces. *Annu. Rev. Phys. Chem.* **2002**, *53*, 319–348.
- (9) Stamenkovic, V. R.; Fowler, B.; Mun, B. S.; Wang, G.; Ross, P. N.; Lucas, C. A.; Marković, N. M. Improved Oxygen Reduction Activity on Pt₃Ni(111) via Increased Surface Site Availability. *Science* **2007**, *315*, 493–497.

- (10) Stephens, I. E. L.; Bondarenko, A. S.; Perez-Alonso, F. J.; Calle-Vallejo, F.; Bech, L.; Johansson, T. P.; Jepsen, A. K.; Frydendal, R.; Knudsen, B. P.; Rossmeisl, J. et al. Tuning the Activity of Pt(111) for Oxygen Electroreduction by Subsurface Alloying. *J. Am. Chem. Soc.* **2011**, *133*, 5485–5491.
- (11) Mohsenzadeh, A.; Richards, T.; Bolton, K. DFT study of the water gas shift reaction on Ni(111), Ni(100) and Ni(110) surfaces. *Surface Science* **2016**, *644*, 53–63.
- (12) Tao, F.; Grass, M. E.; Zhang, Y.; Butcher, D. R.; Renzas, J. R.; Liu, Z.; Chung, J. Y.; Mun, B. S.; Salmeron, M.; Somorjai, G. A. Reaction-Driven Restructuring of Rh-Pd and Pt-Pd Core-Shell Nanoparticles. *Science* **2008**, *322*, 932–934.
- (13) Tao, F.; Dag, S.; Wang, L.-W.; Liu, Z.; Butcher, D. R.; Bluhm, H.; Salmeron, M.; Somorjai, G. A. Break-Up of Stepped Platinum Catalyst Surfaces by High CO Coverage. *Science* **2010**, *327*, 850–853.
- (14) Tao, F. F.; Salmeron, M. In Situ Studies of Chemistry and Structure of Materials in Reactive Environments. *Science* **2011**, *331*, 171–174.
- (15) Michalka, J. R.; McIntyre, P. W.; Gezelter, J. D. Molecular Dynamics Simulations of the Surface Reconstructions of Pt(557) and Au(557) under Exposure to CO. *J. Phys. Chem. C* **2013**, *117*, 14579–14587.
- (16) Michalka, J. R.; Gezelter, J. D. Island Formation on Pt/Pd(557) Surface Alloys in the Presence of Adsorbed CO: A Molecular Dynamics Study. *J. Phys. Chem. C* **2015**, *119*, 14239–14247.
- (17) Kim, J.; Noh, M. C.; Doh, W. H.; Park, J. Y. Thermal Evolution and Instability of CO-Induced Platinum Clusters on the Pt(557) Surface at Ambient Pressure. *J. Am. Chem. Soc.* **2016**, 1110–1113.
- (18) Eren, B.; Zherebetsky, D.; Patera, L. L.; Wu, C. H.; Bluhm, H.; Africh, C.; Wang, L.-

- W.; Somorjai, G. A.; Salmeron, M. Activation of Cu(111) surface by decomposition into nanoclusters driven by CO adsorption. *Science* **2016**, *351*, 475–478.
- (19) Balmes, O.; Prevot, G.; Torrelles, X.; Lundgren, E.; Ferrer, S. Diatomic Steps in Pt(997) Surfaces Are Better Catalysts than Monatomic Steps for the CO Oxidation Reaction near Atmospheric Pressure. *ACS Catalysis* **2016**, *6*, 1285–1291.
- (20) McClellan, M. R.; Gland, J. L.; McFeeley, F. Carbon monoxide adsorption on the kinked Pt(321) surface. *Surf. Sci.* **1981**, *112*, 63 – 77.
- (21) Bray, J.; Smith, J.; Schneider, W. Coverage-Dependent Adsorption at a Low Symmetry Surface: DFT and Statistical Analysis of Oxygen Chemistry on Kinked Pt(321). *Top. Catal.* **2014**, *57*, 89–105.
- (22) Bray, J. M.; Schneider, W. F. Potential Energy Surfaces for Oxygen Adsorption, Dissociation, and Diffusion at the Pt(321) Surface. *Langmuir* **2011**, *27*, 8177–8186.
- (23) Xu, J.; Jr., J. T. Y. Terrace width effect on adsorbate vibrations: a comparison of Pt(335) and Pt(112) for chemisorption of CO. *Surface Science* **1995**, *327*, 193 – 201.
- (24) Yates, J., John T. Surface chemistry at metallic step defect sites. *J. Vac. Sci. Technol. A* **1995**, *13*, 1359.
- (25) Kim, C. S.; Korzeniewski, C. Vibrational Coupling as a Probe of Adsorption at Different Structural Sites on a Stepped Single-Crystal Electrode. *Anal. Chem.* **1997**, *69*, 2349–2353.
- (26) Kresse, G.; Hafner, J. *Ab initio* molecular dynamics for liquid metals. *Phys. Rev. B* **1993**, *47*, 558–561.
- (27) Kresse, G.; Hafner, J. *Ab initio* molecular dynamics for open-shell transition metals. *Phys. Rev. B* **1993**, *48*, 13115–13118.
- (28) Kresse, G.; Hafner, J. *Ab initio* molecular-dynamics simulation of the liquid-metal amorphous-semiconductor transition in germanium. *Phys. Rev. B* **1994**, *49*, 14251–14269.

- (29) Car, R.; Parrinello, M. Unified Approach for Molecular Dynamics and Density-Functional Theory. *Phys. Rev. Lett.* **1985**, *55*, 2471–2474.
- (30) Izvekov, S.; Philpott, M. R.; Eglitis, R. I. Ab Initio Simulation of Metal Cluster Surrounded by Electrolyte. *J. Electrochem. Soc.* **2000**, *147*, 2273–2278.
- (31) Guidelli, R.; Schmickler, W. Recent developments in models for the interface between a metal and an aqueous solution. *Electrochimic. Acta* **2000**, *45*, 2317 – 2338.
- (32) Foiles, S. M.; Baskes, M. I.; Daw, M. S. Embedded-Atom-Method Functions for the Fcc Metals Cu, Ag, Au, Ni, Pd, Pt, And Their Alloys. *Phys. Rev. B* **1986**, *33*, 7983.
- (33) Straub, J. E.; Karplus, M. Molecular dynamics study of the photodissociation of carbon monoxide from myoglobin: Ligand dynamics in the first 10 ps. *Chem. Phys.* **1991**, *158*, 221 – 248.
- (34) Yeo, Y. Y.; Vattuone, L.; King, D. A. Calorimetric heats for CO and oxygen adsorption and for the catalytic CO oxidation reaction on Pt(111). *J. Chem. Phys.* **1997**, *106*, 392–402.
- (35) Kelemen, S.; Fischer, T.; Schwarz, J. The Binding Energy of CO on Clean and Sulfur Covered Platinum Surfaces. *Surf. Sci.* **1979**, *81*, 440–450.
- (36) Deshlahra, P.; Conway, J.; Wolf, E. E.; Schneider, W. F. Influence of Dipole–Dipole Interactions on Coverage-Dependent Adsorption: CO and NO on Pt(111). *Langmuir* **2012**, *28*, 8408–8417.
- (37) Korzeniewski, C.; Pons, S.; Schmidt, P. P.; Severson, M. W. A theoretical analysis of the vibrational spectrum of carbon monoxide on platinum metal electrodes. *J. Chem. Phys.* **1986**, *85*, 4153–4160.
- (38) van Beurden, P.; Verhoeven, H. G. J.; Kramer, G. J.; Thijsse, B. J. Atomistic potential for adsorbate/surface systems: CO on Pt. *Phys. Rev. B* **2002**, *66*, 235409.

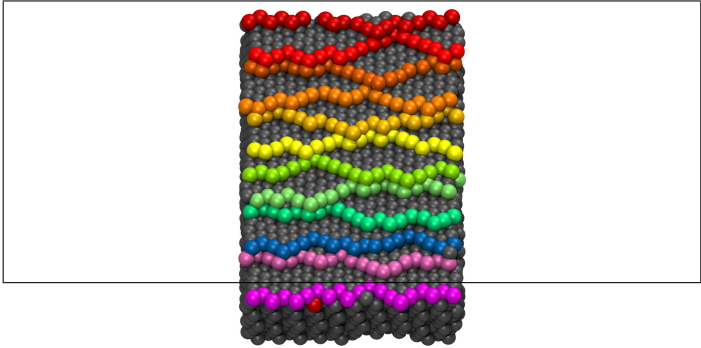
- (39) Deslahra, P.; Wolf, E. E.; Schneider, W. F. A Periodic Density Functional Theory Analysis of CO Chemisorption on Pt(111) in the Presence of Uniform Electric Fields. *J. Phys. Chem. A* **2009**, *113*, 4125–4133.
- (40) Feibelman, P. J.; Hammer, B.; Nørskov, J. K.; Wagner, F.; Scheffler, M.; Stumpf, R.; Watwe, R.; Dumesic, J. The CO/Pt(111) Puzzle. *J. Phys. Chem. B* **2001**, *105*, 4018–4025.
- (41) Mason, S. E.; Grinberg, I.; Rappe, A. M. First-principles extrapolation method for accurate CO adsorption energies on metal surfaces. *Phys. Rev. B* **2004**, *69*, 161401.
- (42) Daw, M. S.; Baskes, M. I. Embedded-atom method: Derivation and application to impurities, surfaces, and other defects in metals. *Phys. Rev. B* **1984**, *29*, 6443–6453.
- (43) Johnson, R. A. Alloy models with the embedded-atom method. *Phys. Rev. B* **1989**, *39*, 12554–12559.
- (44) Daw, M. S. Model of metallic cohesion: The embedded-atom method. *Phys. Rev. B* **1989**, *39*, 7441–7452.
- (45) Plimpton, S. J.; Hendrickson, B. A. Parallel Molecular Dynamics With the Embedded Atom Method. Symposium O – Materials Theory and Modeling. 1992.
- (46) Lu, J.; Szpunar, J. A. Applications of the embedded-atom method to glass formation and crystallization of liquid and glass transition-metal nickel. *Philos. Mag. A* **1997**, *75*, 1057–1066.
- (47) Alemany, M. M. G.; Rey, C.; Gallego, L. J. Transport coefficients of liquid transition metals: A computer simulation study using the embedded atom model. *J. Chem. Phys.* **1998**, *109*, 5175–5176.
- (48) Voter, A. F. In *Intermetallic Compounds: Principles and Practice*; Westbrook, J., Fleischer, R., Eds.; John Wiley & Sons Ltd, 1994; Chapter The Embedded-Atom Method, pp 77–90.

- (49) Finnis, M. W.; Sinclair, J. E. A simple empirical N-body potential for transition metals. *Philos. Mag. A* **1984**, *50*, 45–55.
- (50) Sutton, A. P.; Chen, J. Long-range Finnis–Sinclair potentials. *Phil. Mag. Lett.* **1990**, *61*, 139–146.
- (51) Qi, Y.; Çağın, T.; Kimura, Y.; Goddard, W. A. Molecular-dynamics simulations of glass formation and crystallization in binary liquid metals: Cu-Ag and Cu-Ni. *Phys. Rev. B* **1999**, *59*, 3527–3533.
- (52) Mishin, Y.; Farkas, D.; Mehl, M. J.; Papaconstantopoulos, D. A. Interatomic potentials for monoatomic metals from experimental data and *ab initio* calculations. *Phys. Rev. B* **1999**, *59*, 3393–3407.
- (53) Chui, Y. H.; Chan, K. Y. Analyses of surface and core atoms in a platinum nanoparticle. *Phys. Chem. Chem. Phys.* **2003**, *5*, 2869–2874.
- (54) Wang, G.; Van Hove, M. A.; Ross, P. N.; Baskes, M. I. Surface Structures of Cubo-Octahedral PtMo Catalyst Nanoparticles from Monte Carlo Simulations. *J. Phys. Chem. B* **2005**, *109*, 11683–11692.
- (55) Medasani, B.; Park, Y. H.; Vasiliev, I. Theoretical study of the surface energy, stress, and lattice contraction of silver nanoparticles. *Phys. Rev. B* **2007**, *75*, 235436.
- (56) Belonoshko, A. B.; Ahuja, R.; Eriksson, O.; Johansson, B. Quasi *ab initio* molecular dynamic study of Cu melting. *Phys. Rev. B* **2000**, *61*, 3838–3844.
- (57) Sankaranarayanan, S. K. R. S.; Bhethanabotla, V. R.; Joseph, B. Molecular dynamics simulation study of the melting of Pd-Pt nanoclusters. *Phys. Rev. B* **2005**, *71*, 195415.
- (58) Sankaranarayanan, S. K. R. S.; Bhethanabotla, V. R.; Joseph, B. Molecular dynamics simulation study of the melting and structural evolution of bimetallic Pd-Pt nanowires. *Phys. Rev. B* **2006**, *74*, 155441.

- (59) Shastry, V.; Farkas, D. Molecular statics simulation of fracture in alpha-iron. *Modelling Simulation Mater. Sci. Eng.* **1996**, *4*, 473.
- (60) Shastry, V.; Farkas, D. Atomistic simulation of fracture in CoAl and FeAl. *Intermetallics* **1998**, *6*, 95 – 104.
- (61) Mishin, Y.; Mehl, M. J.; Papaconstantopoulos, D. A.; Voter, A. F.; Kress, J. D. Structural stability and lattice defects in copper: *Ab initio*, tight-binding, and embedded-atom calculations. *Phys. Rev. B* **2001**, *63*, 224106.
- (62) Becquart, C.; Kim, D.; Rifkin, J.; Clapp, P. Fracture properties of metals and alloys from molecular dynamics simulations. *Mater. Sci. Eng.* **1993**, *170*, 87 – 94.
- (63) Shibata, T.; Bunker, B. A.; Zhang, Z.; Meisel, D.; Vardeman, C. F.; Gezelter, J. D. Size-Dependent Spontaneous Alloying of AuAg Nanoparticles. *J. Am. Chem. Soc.* **2002**, *124*, 11989–11996.
- (64) Mishin, Y.; Mehl, M. J.; Papaconstantopoulos, D. A. Embedded-atom potential for $B2$ – NiAl. *Phys. Rev. B* **2002**, *65*, 224114.
- (65) Zope, R. R.; Mishin, Y. Interatomic potentials for atomistic simulations of the Ti-Al system. *Phys. Rev. B* **2003**, *68*, 024102.
- (66) Mishin, Y.; Mehl, M.; Papaconstantopoulos, D. Phase stability in the Fe–Ni system: Investigation by first-principles calculations and atomistic simulations. *Acta Materialia* **2005**, *53*, 4029 – 4041.
- (67) Tyson, W.; Miller, W. Surface free energies of solid metals: Estimation from liquid surface tension measurements. *Surf. Sci.* **1977**, *62*, 267 – 276.
- (68) De Boer, F. R.; Boom, R.; Mattens, W. C. M.; Miedema, A. R.; Niessen, A. K. *Cohesion in Metals: Transition Metal Alloys*; Cohesion and Structure; Elsevier: Amsterdam, 1988; Vol. 1.

- (69) Galeev, T. K.; Bulgakov, N. N.; Savelieva, G. A.; Popova, N. M. Surface Properties of Platinum and Palladium. *React. Kinet. Catal. Lett.* **1980**, *14*, 61–65.
- (70) Vitos, L.; Ruban, A.; Skriver, H.; Kollár, J. The surface energy of metals. *Surf. Sci.* **1998**, *411*, 186 – 202.
- (71) Chetty, N.; Couling, V. W. Measurement of the electric quadrupole moment of CO. *J. Chem. Phys.* **2011**, *134*.
- (72) Noro, M. G.; Frenkel, D. Extended corresponding-states behavior for particles with variable range attractions. *J. Chem. Phys.* **2000**, *113*.
- (73) Hört, P.; Ruff, P.; Schäfer, R. A Temperature Dependent Investigation of the Adsorption of CO on Pt(111) using Low-Temperature Single Crystal Adsorption Calorimetry. *Surf. Sci.* **2015**, 66–69.
- (74) Myshlyavtsev, A. V.; Stishenko, P. V. Potential of lateral interactions of CO on Pt (111) fitted to recent STM images. *Surf. Sci.* **2015**, 51–57.
- (75) Meineke, M. A.; Vardeman, C. F.; Lin, T.; Fennell, C. J.; Gezelter, J. D. OOPSE: An object-oriented parallel simulation engine for molecular dynamics. *J. Comput. Chem.* **2005**, *26*, 252–271.
- (76) Gezelter, J. D.; Michalka, J.; Kuang, S.; Marr, J.; Stocker, K.; Li, C.; Vardeman, C. F.; Lin, T.; Fennell, C. J.; Sun, X. et al. OpenMD, an Open Source Engine for Molecular Dynamics. Available at <http://openmd.org>.
- (77) Calle-Vallejo, F.; Tymoczko, J.; Colic, V.; Vu, Q. H.; Pohl, M. D.; Morgenstern, K.; Loffreda, D.; Sautet, P.; Schuhmann, W.; Bandarenka, A. S. Finding optimal surface sites on heterogeneous catalysts by counting nearest neighbors. *Science* **2015**, *350*, 185–189.

Graphical TOC Entry



Supporting information for:
CO-Induced Restructuring on Stepped Pt
Surfaces: A Molecular Dynamics Study

Joseph R. Michalka,^{†,‡} Andrew P. Latham,[†] and J. Daniel Gezelter^{*,†}

[†]Department of Chemistry and Biochemistry

University of Notre Dame

251 Nieuwland Science Hall

Notre Dame, Indiana 46556

[‡]Department of Chemistry and Physics

Southwest Baptist University

Wheeler Science Facility

Bolivar, Missouri 65613

E-mail: gezelter@nd.edu

Phone: (574) 631-7595

Step-wandering during the simulations can interfere with easy interpretation of the generalized coordination figures. Figure S1 provides an additional ideal surface to complement the ideal Pt(321) GCN distribution shown in the main paper. The Pt(557) surface has straight step edges, and the GCN distribution therefore has fewer peaks than the Pt(321) surface.

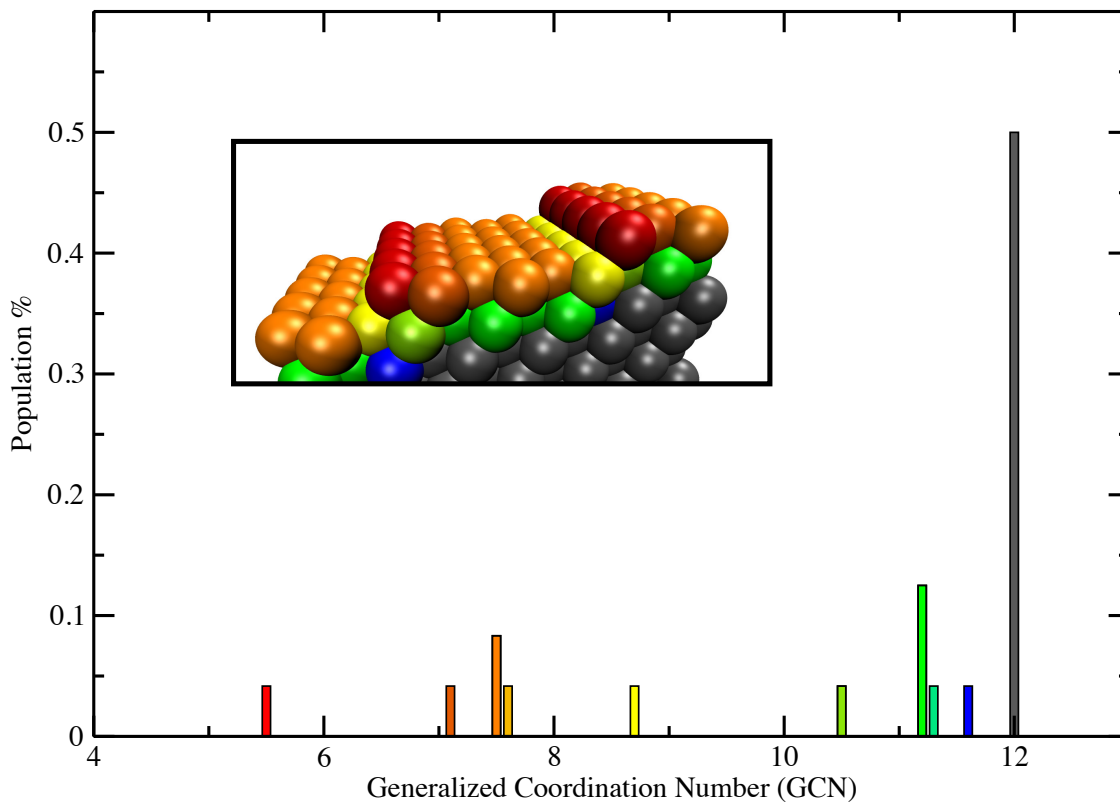


Figure S1: The generalized coordination number of an ideal Pt(557) system colored to match the inset structure. Other than the bulk (GCN = 12), the ideal (557) surface displays a variety of coordination environments at its surface. The under-coordinated edge atoms (red) have the lowest GCN, where the plateau atoms have GCN values around the ideal (111) surface number of 7.5. Subsurface atoms (yellow, greens, and blues) have a larger GCN than the surface, but are still less coordinated than the bulk.

The Pt(557) surface did not exhibit step doubling in the simulations reported in this work, so the distribution of generalized coordination numbers did not undergo significant changes, as shown in Figure S2.

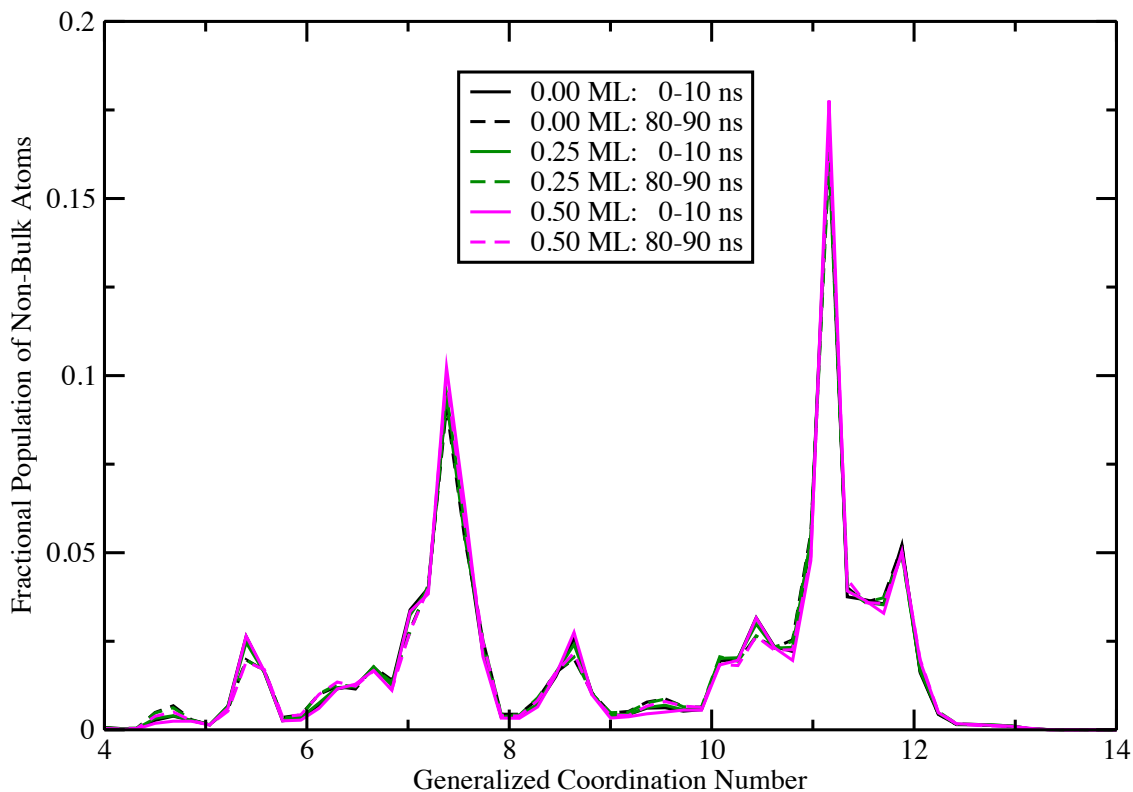


Figure S2: The distribution of generalized coordination numbers (GCN) for the near-surface atoms of the Pt(557) LS systems. Solid lines represent the averaged GCN during the first 10 ns of simulation time, while dotted lines correspond to the last 10 ns. Black, green and magenta lines depict the 0, 0.25, and 0.5 ML systems respectively. Except for a small decrease at GCN values of 5.5 and 10.5, minimal changes were observed.

On the Pt(765) surfaces, reconstruction on only the MS 0.5 ML system was observed, but none of the other surfaces exhibited reconstruction beyond step wandering. The slight increase in the peak at GCN ~ 7.5 suggests that this measurement is sensitive to relatively minor surface reconstruction, like the step-edge doubling and disappearance highlighted in Figure S6.

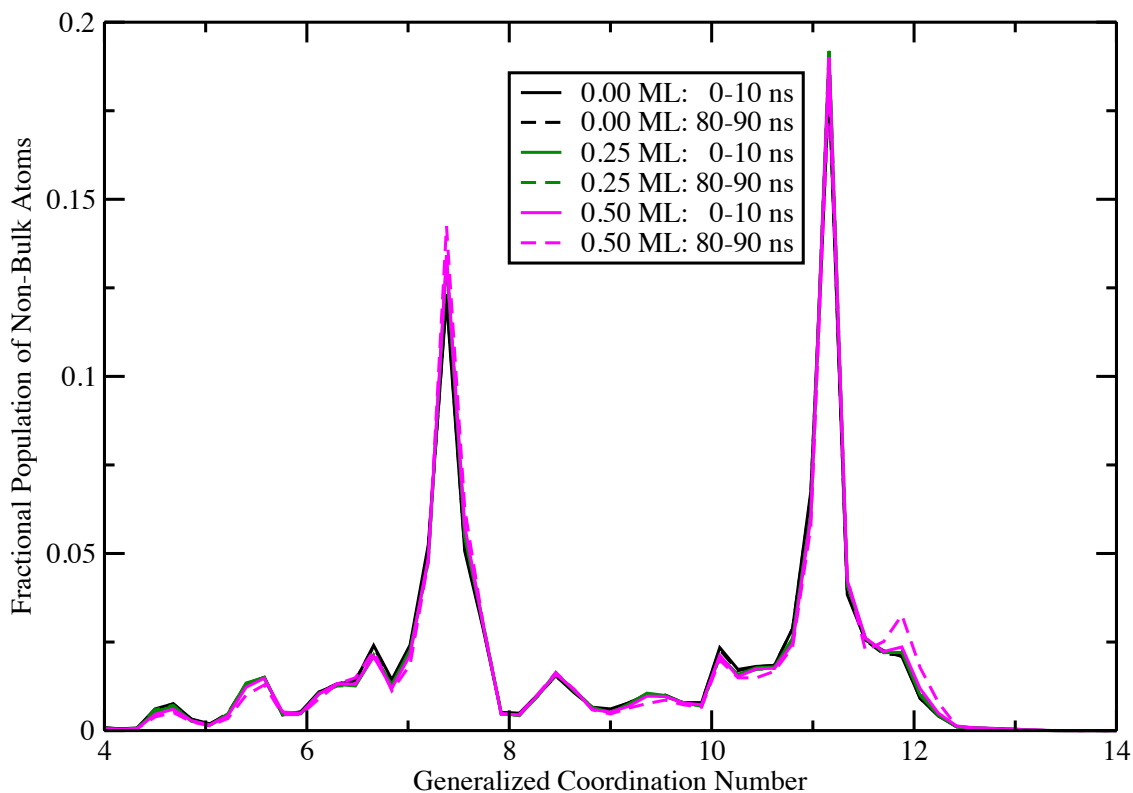


Figure S3: The distribution of generalized coordination numbers (GCN) for the near-surface atoms of the Pt(765) MS systems. Line styles and colors are the same as in Fig. S2. The increasing peak heights seen at GCN ~ 7.5 and 11.8 capture the doubling process explored in Figure S6.

The increase in the peak height at $\text{GCN} \sim 6.8$ for the 0 and 0.5 ML LS systems appears to be capturing the loss of the clean (765) surface. In contrast, the 0.25 ML LS system only exhibited step-edge wandering, but generally maintained the originally-displayed edges.

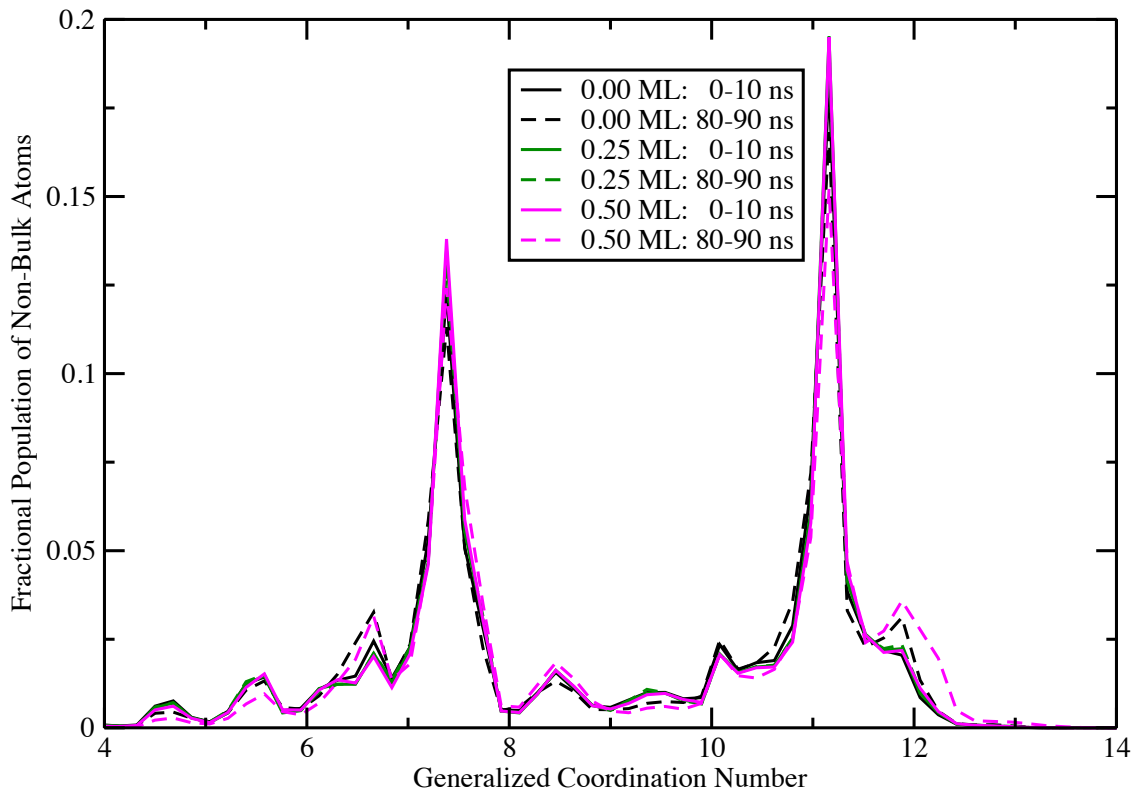


Figure S4: The distribution of generalized coordination numbers (GCN) for the near-surface atoms of the Pt(765) LS systems. Line styles and colors are the same as in Fig. S2. The increasing peak heights seen at $\text{GCN} \sim 6.8$ and 11.8 for the 0.0 and 0.5 ML systems capture the disruption mentioned in the main text.

The Pt(112) systems explored in this study were run at temperatures close to a surface melting transition. One reflection of this is the partial sinking of step edges into the surface. In Figure S5, a few of the edges maintained $\{100\}$ step facets and were a source for adatoms. However, the sunken steps rarely ejected adatoms, and for the majority of the simulation, exhibited minimal movement on the surface.

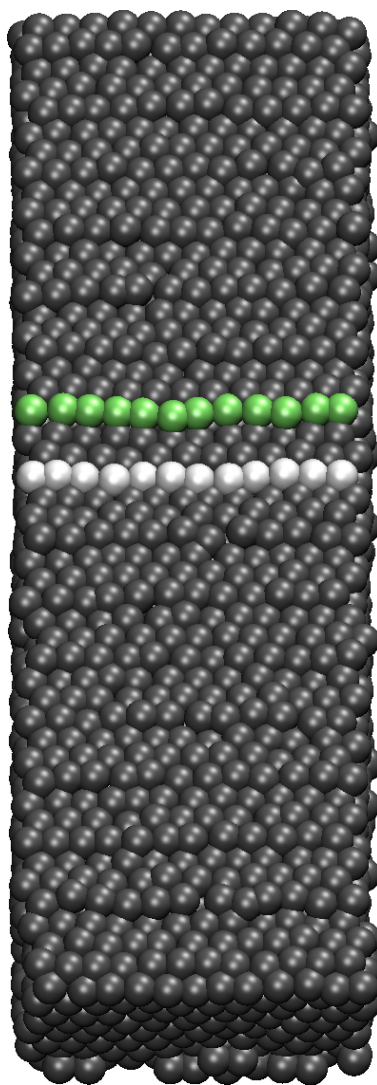


Figure S5: The Pt(112) systems have a large surface energy, and exhibited restructuring that resulted in many of the $\{100\}$ steps sinking into the surface (white) and shifting half a unit-cell to display a sunken $\{111\}$ step edge. A few step edges (green) retained $\{100\}$ step edge morphology and were the primary source for adatom formation and edge wandering.

The kinked edges and large plateaus of the Pt(765) systems help distinguish which surface attributes were most important in encouraging or hindering surface reconstruction. No clear step-doubling occurred on these surfaces despite a significant amount of step-wandering. On the 0.5 ML MS system shown in Fig. S6, what were originally two separate steps, coalesced into a single step located at an intermediate distance between the original step edges. A portion of each step sunk into the surface allowing the two remaining plateaus to meet up to form a single step edge.

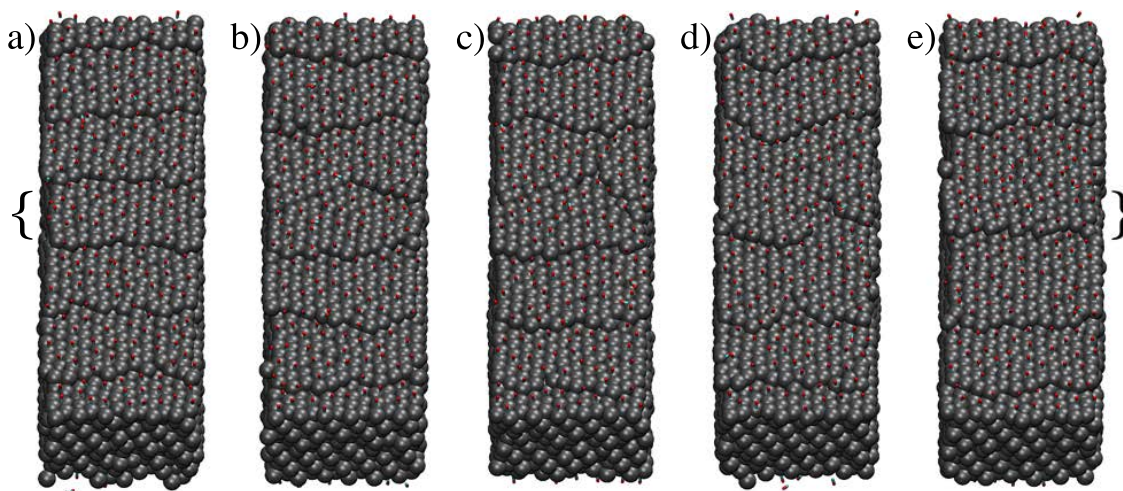


Figure S6: The Pt(765)-MS 0.5 ML system (a) 0 ns, (b) 33.4 ns, (c) 50.2 ns, (d) 75.1 ns, (e) and 100 ns after exposure to CO. The step-edges indicated with a bracket in (a) approach each other while sinking into the surface. The result is a step-edge that is between the starting points of both parents, but which is only one atom elevated from the surface.